

Wetting under nonequilibrium conditionsH. Hinrichsen,^{1,2} R. Livi,³ D. Mukamel,¹ and A. Politi⁴¹*Department of Physics of Complex Systems, Weizmann Institute of Science, Rehovot 76100, Israel*²*Theoretische Physik, Fachbereich 8, Bergische Universität Wuppertal, 42097 Wuppertal, Germany*³*Dipartimento di Fisica, Università di Firenze, INFN UdR di Firenze and INFN Sezione di Firenze, via Sansone 1, 50019 Sesto Fiorentino, Italy*⁴*Istituto Nazionale di Ottica Applicata, Largo E. Fermi 6, Firenze, Italy and INFN UdR di Firenze, via Sansone 1, 50019 Sesto Fiorentino, Italy*

(Received 6 May 2003; published 20 October 2003)

We report a detailed account of the phase diagram of a recently introduced model for nonequilibrium wetting in $(1+1)$ dimensions [H. Hinrichsen, R. Livi, D. Mukamel, and A. Politi, *Phys. Rev. Lett.* **79**, 2710 (1997)]. A mean-field approximation is shown to reproduce the main features of the phase diagram, while providing indications for the behavior of the wetting transition in higher dimensions. The mean-field phase diagram is found to exhibit an extra transition line which does not exist in $(1+1)$ dimensions. The line separates a phase in which the interface height distribution decays exponentially at large heights from a superexponentially decaying phase. Implications to wetting in dimensions higher than $(1+1)$ are discussed.

DOI: 10.1103/PhysRevE.68.041606

PACS number(s): 68.08.Bc, 05.70.Ln, 05.70.Np

I. INTRODUCTION

Wetting phenomena occur in a large variety of experiments, where a planar substrate is exposed to a gas phase under thermal equilibrium conditions. Generally, “wetting” refers to a situation where a bulk phase (α) in contact with a substrate coexists with a layer of a different phase (β) which is preferentially attracted to the surface of the substrate. By changing physical parameters such as temperature and chemical potential, the system may undergo a wetting transition from a nonwet phase, where the thickness of the layer stays finite, to a wet phase, where the layer becomes macroscopic.

The phase diagram associated with the surface layer could be rather complex exhibiting a variety of surface phase transitions, prewetting phenomena, and multicritical behavior [1,2]. For example, by increasing the temperature T while moving along the α - β coexistence curve, a wetting transition may take place at a temperature T_w , beyond which the thickness of the layer becomes infinite. Usually this transition is of first order, although in certain models the transition is continuous, and is then referred to as continuous wetting. On the other hand, when the chemical potential difference between the two phases is varied, moving towards the coexistence curve at $T > T_w$, a different type of transition takes place in which the thickness of the layer diverges. This phenomenon is known as complete wetting.

In many experimental situations, it is reasonable to assume that a wetting stationary layer is in thermal equilibrium. In fact, methods of equilibrium statistical mechanics turned out to be very successful in a large variety of theoretical and experimental studies (for a review, see Ref. [1]). Within this approach, a wetting transition is usually considered as the unbinding of an interface from a wall. The interface configuration is described by a function $h(\mathbf{x})$ which gives the height of the interface at point \mathbf{x} on the substrate. One then introduces an effective Hamiltonian of the form [3]

$$\mathcal{H} = \int d^{d-1}x \left[\frac{\sigma}{2} (\nabla h)^2 + V(h(\mathbf{x})) \right], \quad (1)$$

where σ is the effective surface tension of the α - β interface, $V(h)$ is a potential accounting for the interaction between the wall and the interface, and $d-1$ is the interface dimension. In the nonwet phase the potential V contains an attractive component which binds the interface to the wall. Assuming thermal equilibrium, the probability of finding the interface in a certain configuration is then given by the canonical distribution

$$P[h] \sim \exp(-\beta \mathcal{H}[h]). \quad (2)$$

As the parameters describing the system are varied, the attractive component of the potential may become weaker so that it is no longer able to bind the interface, leading to a wetting transition.

In order to study wetting phenomena under thermal equilibrium conditions, one usually introduces a stochastic Langevin equation corresponding to the effective Hamiltonian (1). This Langevin dynamics should reproduce equilibrium distribution (2) in the limit $t \rightarrow \infty$. Since many different dynamical rules may approach the same stationary state, this condition does not fully determine the form of the Langevin equation. However, assuming short-range interactions and keeping only the most relevant terms in the renormalization group sense, one is led to the Edwards-Wilkinson equation with a potential [4]

$$\frac{\partial h(\mathbf{x}, t)}{\partial t} = \sigma \nabla^2 h(\mathbf{x}, t) - \frac{\partial V(h(\mathbf{x}, t))}{\partial h(\mathbf{x}, t)} + \zeta(\mathbf{x}, t), \quad (3)$$

where $\zeta(\mathbf{x}, t)$ is a zero-average Gaussian noise field with a variance

$$\langle \zeta(\mathbf{x}, t) \zeta(\mathbf{x}', t') \rangle = 2\Gamma \delta^{d-1}(\mathbf{x} - \mathbf{x}') \delta(t - t'), \quad (4)$$

and a noise amplitude $\Gamma = k_B T$. This Langevin equation has the same symmetry properties as Hamiltonian (1), namely, it is invariant under translations, rotations, and reflections in space. Apart from the potential term, the equation is also invariant under shifts $h \rightarrow h + a$ and reflections $h \rightarrow -h$. Moreover, it can be shown that this type of Langevin dynam-

ics obeys *detailed balance* and relaxes towards equilibrium distribution (2) in the bound phase.

Wetting phenomena may also take place in many systems under nonequilibrium conditions. For example, in growth processes such as molecular beam epitaxy or others, a layer is grown on a substrate, whose properties depend on the growth conditions. By varying these conditions, one expects wetting phenomena to take place. Here, unlike the equilibrium case, the dynamics does not obey detailed balance, leading to a rather different class of wetting phenomena.

The simplest way to study nonequilibrium wetting on the level of the Langevin equation is to introduce a nonlinear term in Eq. (3), leading to a Kardar-Parisi-Zhang (KPZ) equation with a potential [5]

$$\frac{\partial h(\mathbf{x},t)}{\partial t} = \sigma \nabla^2 h(\mathbf{x},t) - \frac{\partial V(h(\mathbf{x},t))}{\partial h(\mathbf{x},t)} + \lambda [\nabla h(\mathbf{x},t)]^2 + \zeta(\mathbf{x},t). \quad (5)$$

It is important to note that this nonlinear term is a relevant perturbation of the underlying field theory, i.e., even if λ is very small, it will be amplified under renormalization group transformations, driving the system away from thermal equilibrium.

Recently, a simple solid-on-solid (SOS) model for non-equilibrium wetting in (1+1) dimensions was introduced [6,7]. The model is controlled by an adsorption rate q and a desorption rate p and exhibits a continuous wetting transition at a critical growth rate $q_c(p)$. The wetting transition is related to the unpinning process of an interface from a substrate and may be described by the KPZ equation (5). The model has then been generalized to include a short-range interaction between the interface and the substrate [8]. This was done by introducing a modified growth rate q_0 at the substrate level. This results in a contact interaction between the interface and the substrate, which is attractive for $q_0 < q$ and repulsive for $q_0 > q$. It was found that sufficiently strong attractive interaction modifies the nature of the wetting transition, making it first order. In addition, it has been demonstrated that there exists an extended region in the phase diagram, where the pinned and the moving phases *coexist* in the sense that the transition time from the pinned to the moving phase grows exponentially with the system size so that the two phases become stable in the thermodynamic limit. It should be emphasized that this kind of phase coexistence, which has also been observed in the past in other models [9–12], can only occur in nonequilibrium systems.

Some of these results have been confirmed by numerical and mean-field studies of KPZ type models [13,14]. In particular, by adding a repulsive interaction between the interface and the substrate, a crossover from a continuous to a first-order wetting transition was found. Nonequilibrium wetting phenomena have also been studied recently in models of growing magnetic domains [15].

In this paper, we present a detailed account of the phase diagram of the SOS model in (1+1) dimensions. In order to get some indication on the behavior of the model in higher dimensions, we introduce a mean-field approximation for the model and study the resulting phase diagram and the dy-

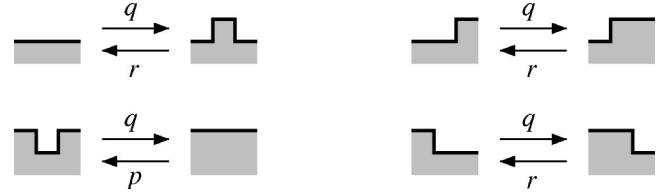


FIG. 1. Deposition and evaporation processes in the bulk. At the hard-core wall at zero height (not shown here), evaporation is forbidden and the deposition rate q is replaced by a modified deposition rate q_0 in order to take the interaction between substrate and surface layer into account.

namical behavior of the interface. It is found that the mean-field approximation reproduces the main qualitative features of the phase diagram obtained in 1+1 dimensions. In addition, a new feature is found in the pinned phase. By studying the height distribution of the pinned interface, two distinct types of behavior are discovered upon varying the dynamical parameters of the model: in one regime the distribution decays superexponentially with the height, while in the other the decay is exponential. The two regimes are separated by a prewetting transition line. Relevance of this phase diagram to wetting phenomena in dimensions higher than (1+1) is considered.

The paper is organized as follows. In Sec. II, we recall the definition of the SOS model and summarize its properties. The special case $p=1$, where the model is exactly solvable, is discussed in detail in Sec. III. The mean-field approximation, which is the main focus of the present work, is presented and analyzed in Sec. IV. The paper ends with concluding remarks in Sec. V.

II. DEFINITION AND PROPERTIES OF THE MODEL

The SOS model defined in Ref. [7] is probably the simplest model which follows the spirit of Eq. (5). It is defined on a one-dimensional lattice with N sites and periodic boundary conditions, where each site i is associated with an integer variable h_i describing the local height of the interface. The repulsive part of the potential $V(h)$ is implemented as a hard-core wall at zero height, restricting the heights h_i to be non-negative. Thus $h_i = 0, 1, 2, \dots$. Moreover, an effective surface tension is introduced by imposing the restricted solid-on-solid (RSOS) condition

$$|h_i - h_{i\pm 1}| \leq 1. \quad (6)$$

The model evolves randomsequentially by choosing a random site and carrying out one of the following processes (see Fig. 1).

(a) Deposition of an atom on the substrate with rate q_0 :

$$h_i = 0 \rightarrow h_i = 1. \quad (7)$$

(b) Deposition of an atom on top of already deposited islands with rate q :

$$h_i \rightarrow h_i + 1 \quad \text{if } h_i \geq 1. \quad (8)$$

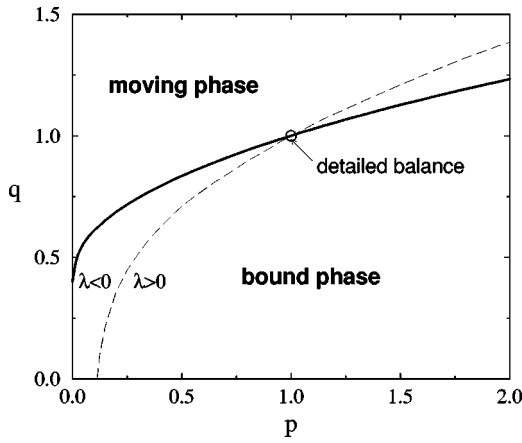


FIG. 2. Phase diagram of the wetting model for $q_0 = q$. The second-order wetting transition is represented as a solid line. The dashed line indicates where the coefficient λ of the nonlinear term in the KPZ equation effectively vanishes. For $p = 1$ the dynamical rules obey detailed balance (see text).

(c) Evaporation of an atom at the edge of a terrace with rate r :

$$h_i \rightarrow \min(h_{i-1}, h_i, h_{i+1}). \quad (9)$$

(d) Evaporation of an atom in the middle of a plateau with rate p :

$$h_i \rightarrow h_i - 1 \quad \text{if } h_{i-1} = h_i = h_{i+1} > 0. \quad (10)$$

If the selected process would violate the restrictions $h_i \geq 0$ or $|h_i - h_{i\pm 1}| \leq 1$, the attempted move is abandoned and a new site i is selected. Each attempted update corresponds to a time increment $\Delta t = 1/N$. Since one of the four rates can be chosen freely by rescaling time, we set $r = 1$. Thus the model is controlled by three parameters, namely, a growth rate q , a desorption rate p , and a special growth rate q_0 at the substrate which accounts for an additional short-range interaction between the substrate and the wetting layer.

The model can be easily generalized to higher dimensions. Note that in this case it is possible to introduce different evaporation rates for various types of edge sites, e.g., linear edges and corner sites. For simplicity, we will assume that all rates for evaporation at edges are equal to 1. In this case, the model can simply be generalized to higher dimensions by including all nearest neighbors in Eqs. (9) and (10).

A. Properties for $q_0 = q$

Let us first consider the case without interactions between substrate and wetting layer, i.e., $q_0 = q$. In this case, the presence of a hard-core wall at zero height leads to a *continuous* phase transition between a bound and a moving phase (see Fig. 2). The phase transition line $q_c(p)$ is determined by a vanishing propagation velocity of a freely evolving interface. For $q < q_c$ the interface moves downward until it fluctuates close to the wall, while for $q > q_c$ the propagation velocity is positive and the interface detaches from the wall. Obviously, this transition takes place even in finite systems with a criti-

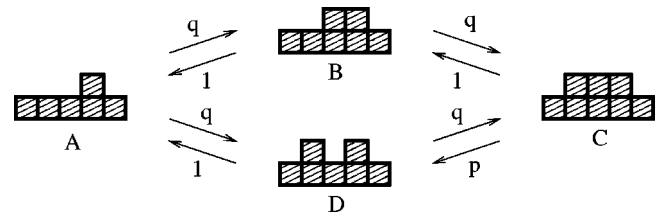


FIG. 3. Example of a closed cycle of deposition and evaporation processes, showing that detailed balance can only be established if $p = 1$.

cal threshold depending on N . We note that for $p = 0$, where evaporation from the middle of plateaus is forbidden, the interface velocity in the bulk cannot be negative so that in this case the transition relies on a different mechanism [6].

One can easily verify that dynamical rules (7)–(10) do not generally satisfy detailed balance. To this end we consider the closed cycle of deposition and evaporation processes, as shown in Fig. 3. Let the statistical weights of these configurations in the steady state be P_A, P_B, P_C , and P_D . Obviously detailed balance implies

$$q^2 P_A = q P_B = P_C = \frac{q}{p} P_D = \frac{q^2}{p} P_A. \quad (11)$$

These equations can only be satisfied if $p = 1$ (as already anticipated, r is assumed to be equal to 1 without any loss of generality). This special case will be discussed in more detail in Sec. III.

The two parameters p and q can be used to control $\partial V / \partial h$ and λ in the KPZ equation (5). In the case of detailed balance, where a bound interface is thermally equilibrated, the coefficient λ is expected to vanish. This can be verified by comparing the propagation velocities of a horizontal and an artificially tilted interface far away from the wall. The line, where both velocities coincide, is shown as a dashed line in Fig. 2. As expected, it crosses the phase transition line exactly at the point $p = q = 1$, where detailed balance is satisfied.

Moving away from this point, we can therefore study the crossover from equilibrium to nonequilibrium wetting. Numerical simulations suggested that the transitions for $p < 1$ and $p > 1$ are associated with different sets of critical exponents [7]. These findings are in accordance with results obtained by Muñoz and Hwa [5], who showed that the scaling properties of a KPZ interface interacting with a wall depend on the sign of λ .

B. Properties for $q_0 < q$

In most experimental applications the wetting layer interacts with the substrate, giving rise to an additional short-range force at the bottom layer which may be either attractive or repulsive. In the present model such a force can be taken into account by introducing a different growth rate q_0 for deposition at zero height. The influence of this parameter was studied in detail in Ref. [8]. Since q_0 does not influence the propagation velocity of the interface far away from the wall, the location of the transition line, along which the mov-

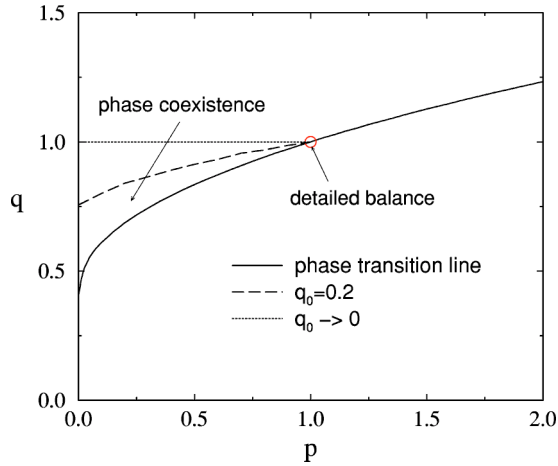


FIG. 4. Phase coexistence region in the phase diagram for small values of q_0 .

ing phase is stable, remains unchanged. However, if q_0 is smaller than a certain threshold q_0^* , the attractive interaction is so strong as to stabilize the bound phase even when the free interface would grow. In other words, for very low values of q_0 , there exists an extended region in the phase diagram where the bound and the moving phase *coexist* in the sense that the transition time from the bound to the moving phase grows exponentially with the systems size. The upper boundary of the coexistence region depends on q_0 , as shown in Fig. 4.

A thermodynamically stable coexistence of the bound and the moving phase requires a robust mechanism which eliminates large protruding islands in the bound phase. In the present model, this mechanism works as follows. Once an island has been formed by fluctuations, the detached part of the interface quickly grows since $q > q_c$. In the phase coexistence region, where the coefficient λ in the KPZ equation is negative, the island will grow until the slope at the edges exceeds a critical value, where the growth is compensated by the nonlinear term. Afterwards, the pyramidal island shrinks linearly with time until it is eliminated. Therefore, phase coexistence can only occur under nonequilibrium conditions in those regions of the phase diagram where λ is negative. Very recently, the tricritical point and the critical behavior at the upper boundary of the phase coexistence region has been investigated in a discretized KPZ equation with a potential [16].

III. EXACTLY SOLUBLE CASE: $p=1$

A. Detailed balance and transfer matrix approach

We first consider the special case $p=1$, where detailed balance is satisfied. In this case, the stationary probability distribution of the bound interface configurations $\{h_1, \dots, h_N\}$ is given by the canonical ensemble expression corresponding to an energy functional \mathcal{H} :

$$P(h_1, \dots, h_N) = \frac{1}{Z_N} \exp[-\mathcal{H}(h_1, \dots, h_N)]. \quad (12)$$

The partition sum

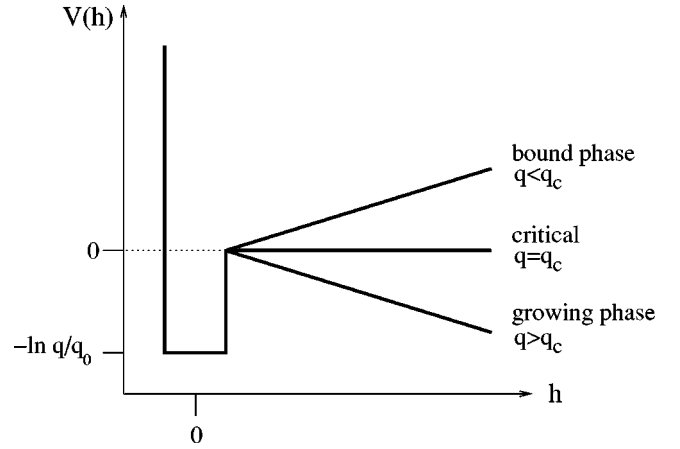


FIG. 5. Schematic drawing of $V(h)$ with a potential well at zero height.

$$Z_N = \sum_{h_1, \dots, h_N} \exp[-\mathcal{H}(h_1, \dots, h_N)] \quad (13)$$

runs over all interface configurations obeying RSOS constraint (6). The energy \mathcal{H} is given by

$$\mathcal{H}(h_1, \dots, h_N) = \sum_{i=1}^N V(h_i), \quad (14)$$

where $V(h)$ is a potential of the form

$$V(h) = \begin{cases} \infty & \text{if } h < 0 \\ -\ln(q/q_0) & \text{if } h = 0 \\ -h \ln(q) & \text{if } h > 0 \end{cases} \quad (15)$$

as sketched in Fig. 5. Therefore, Eq. (12) may be rewritten as

$$P(h_1, \dots, h_N) = Z_N^{-1} q^{(M \sum_{i=1}^N h_i)} (q/q_0)^{(\sum_{i=1}^N \delta_{h_i, 0})}. \quad (16)$$

Note that in this expression $\ln(q)$ plays the role of the chemical potential difference $\Delta\mu/k_B T$ between the wetting layer and the gas phase. Obviously, the transition takes place at $q_c = 1$.

To verify the validity of this probability distribution, it is sufficient to demonstrate that the dynamical rules obey detailed balance with respect to it. In fact, deposition process (8) reduces the probability P by a factor of q , while evaporation processes (9) and (10), which both take place with the same rate, increase P by a factor of $1/q$. Consequently, the probability currents between pairs of configurations compensate each other so that detailed balance is satisfied, proving the validity of the equilibrium ensemble (16). Similarly one can show that detailed balance is also satisfied at the bottom layer. We note that these considerations are only valid in the bound phase $q < 1$, where the probability distribution is stationary. Once the system enters the moving phase, the process is out of equilibrium.

The canonical ensemble can be used to compute the density profile of a bound interface in the case of detailed balance. To this end, we use a transfer matrix formalism intro-

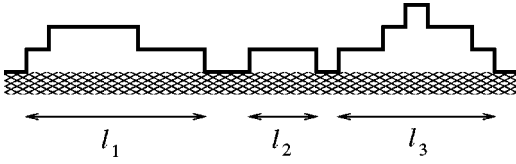


FIG. 6. (1+1)-dimensional interface with island sizes ℓ_1, ℓ_2, ℓ_3 .

where f and g are scaling functions with an appropriate asymptotic behavior. As expected these scaling forms are consistent with the critical exponents $z=2, \alpha=1/2$ of the Edwards-Wilkinson universality class [4].

Another interesting aspect is the stationary distribution $P(\ell)$ of island sizes ℓ in the bound phase (see Fig. 6). In the case of detailed balance, this distribution can be computed exactly. To this end, we introduce the projection operator $P = 1 - |0\rangle\langle 0|$ which projects onto states with nonzero height. Moreover, let $Q = PTP$ be a transfer matrix describing an interface that does not touch the bottom layer. Obviously the distribution $P(\ell)$, which may be interpreted as a first-return probability of the interface to the bottom layer, is given by

$$P(\ell) = \frac{\langle 0|TQ^{\ell-2}T|0\rangle}{\langle 0|T^\ell|0\rangle} \simeq \frac{\langle 0|TQ^{\ell-2}T|0\rangle}{\Lambda^\ell}. \quad (32)$$

Note that the leftmost column and the topmost row of the restricted transfer matrix Q are zero, while all other matrix elements are the same as in Eq. (19). Because of this simple structure, the spectrum of Q is just the spectrum of T multiplied by q combined with a zero mode so that the largest eigenvalue of Q , which dominates the matrix product in Eq. (32), is $q\Lambda$. In the limit $\ell \rightarrow \infty$, we therefore obtain an exponential distribution of the form

$$P(\ell) \sim q^\ell. \quad (33)$$

Therefore, the average island size scales as

$$\bar{\ell} \simeq -\frac{1}{\ln q} \simeq \frac{1}{\epsilon} \quad (34)$$

and diverges at the transition. Since $\rho(0) = 1/\bar{\ell}$, this result is in agreement with Eq. (28).

In order to determine the stationary interface profile $\rho(h)$ in the limit $h \rightarrow \infty$, let us go back to Eq. (23). By assuming that the second and the third term on the left hand side can be neglected, one finds that

$$\phi_h \simeq \frac{1}{\Lambda} q^{h-1/2} \phi_{h-1}, \quad (35)$$

with the corresponding asymptotic solution

$$\phi_h \sim \Lambda^{-h} q^{h^2/2}. \quad (36)$$

Therefore, in the case of detailed balance, the profile of a bound interface decays as a Gaussian for large values of h . Even for $p \neq 1$, where detailed balance is violated, numerical simulations (see Fig. 7) suggest that in (1+1) dimensions

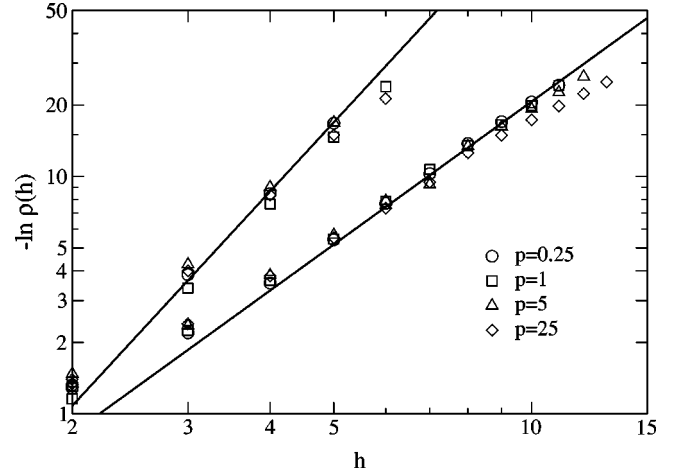


FIG. 7. Numerically determined stationary interface profile of the full model in (1+1) (lower data points) and (2+1) dimensions (upper data points) for different values of p slightly below the critical threshold. The bold lines indicate the slopes 2 and 3, respectively.

the entire bound phase is characterized by Gaussian density profiles.

C. First-order phase transition for small values of q_0

Let us now consider the influence of an attractive force between substrate and wetting layer by taking $q_0 < q$. Obviously, the interface is bound to the wall for $q < 1$, while for $q > 1$ it will tunnel through the potential barrier. This means that the critical point $q_c = 1$ remains unchanged. However, if q_0 is decreased below a certain threshold q_0^* , the attraction is sufficiently strong such that the transition becomes first order.

To demonstrate the crossover to a discontinuous transition in the case of detailed balance, we look for a localized pinned interface solution at the transition point $q = 1$. Assuming an exponential interface profile

$$\phi_h = z^h \quad \text{for } h \geq 1, \quad (37)$$

with some $z < 1$, the eigenvalue problem then reduces to three independent equations

$$\begin{aligned} q_0^{-1} \phi_0 + q_0^{-1/2} z &= \Lambda \phi_0, \\ q_0^{-1/2} \phi_0 + z + z^2 &= \Lambda z, \\ z^{-1} + 1 + z &= \Lambda, \end{aligned} \quad (38)$$

which have the (un-normalized non-negative) solution

$$\phi_0 = q_0^{1/2}, \quad z = \frac{\sqrt{1+2q_0-3q_0^2}}{2(1-q_0)} - \frac{1}{2}, \quad \Lambda = \frac{z+1}{q_0}. \quad (39)$$

Consequently, the stationary density of exposed sites at the bottom layer is

$$\rho(0) = \frac{\phi_0^2}{\sum_{h=0}^{\infty} \phi_h^2} = \frac{q_0}{q_0 + \frac{z^2}{1-z^2}} = \frac{1+q_0-6q_0^2 + \sqrt{1+2q_0-3q_0^2}}{2+4q_0-6q_0^2}, \quad (40)$$

while the densities at higher levels are given by

$$\rho(h) = \frac{\phi_h^2}{\sum_{h=0}^{\infty} \phi_h^2} = \frac{z^{2h}}{q_0 + \frac{z^2}{1-z^2}}. \quad (41)$$

It turns out that the bottom layer density $\rho(0)$ is positive for $q_0 < 2/3$ and vanishes at $q_0 = 2/3$. For $q_0 > 2/3$, however, one has $z > 1$, so that the exponential ansatz $\phi_h = z^h$ is no longer physically meaningful. Hence, in the case of detailed balance, the transition becomes first order at the tricritical point

$$p = q_c = 1, \quad q_0^* = \frac{2}{3}. \quad (42)$$

For $q_0 < \frac{2}{3}$, the potential well is deep enough to bind the critical interface to the wall, leading to an exponentially decaying interface profile. For $q_0 > \frac{2}{3}$, such a localized solution does not exist and the transition becomes continuous.

D. Scaling properties near the tricritical point

The phase diagram for $p = 1$ is shown in Fig. 8. Using the transfer matrix approach, we can show that the critical behavior

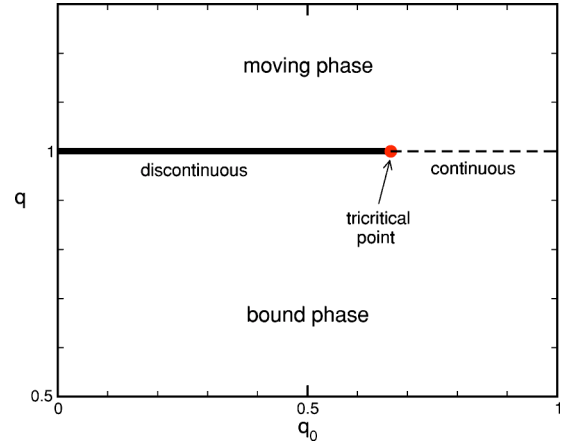


FIG. 8. Phase diagram for $p = 1$ in the (q, q_0) plane.

along the second-order transition line is always the same as the one discussed in Sec. III B. However, in the vicinity of the tricritical point the scaling properties are different. Moreover, they depend on the direction from which the tricritical point is approached.

Let us first consider the case $q = 1$, approaching the tricritical point horizontally from the left along the first-order phase transition line. Using expressions (40) and (41), one can compute the interface height

$$\bar{h} = \sum_{h=0}^{\infty} h \rho(h) = \frac{2q_0}{1+q_0-6q_0^2 + \sqrt{1+2q_0-3q_0^2}} \quad (43)$$

and the squared interface width

$$w^2 = \sum_{h=0}^{\infty} (h - \bar{h})^2 \rho(h) = \frac{2(1+4q_0-3q_0^3 + (q_0^2-3q_0-1)\sqrt{1+2q_0-3q_0^2})}{q_0^2(1+3q_0-3\sqrt{1+2q_0-3q_0^2})^2}. \quad (44)$$

Approaching the tricritical point from the left by increasing q_0 , these quantities scale to lowest order in $\delta = q_0^* - q_0$ as

$$\bar{h} = w = \frac{1}{6\delta}, \quad \rho(0) = 4\delta. \quad (45)$$

On the other hand, if the tricritical point is approached vertically keeping $q_0 = q_0^* = 2/3$ fixed, a numerical diagonalization of the transfer matrix suggests that the asymptotic interface profile crosses over from an exponential to a Gaussian decay. In this case the height, the width, and the bottom layer density are found to scale as

$$\bar{h} \sim w \sim \epsilon^{-1/3}, \quad (46)$$

$$\rho(0) \sim \epsilon^{1/3},$$

where $\epsilon = 1 - q$. Moreover, by keeping the boundary sites fixed at zero height, we can study finite-size scaling at the tricritical point. Evaluating products of the transfer matrix numerically, we find that

$$\bar{h} \sim N^{1/2}, \quad \rho(0) \sim N^{-1/2}. \quad (47)$$

Finally, numerical Monte Carlo simulations at the tricritical point (see Fig. 9) suggest that an initially flat interface roughens in such a way that

$$\bar{h} \sim t^{1/4}, \quad \rho(0) \sim t^{-1/4}. \quad (48)$$

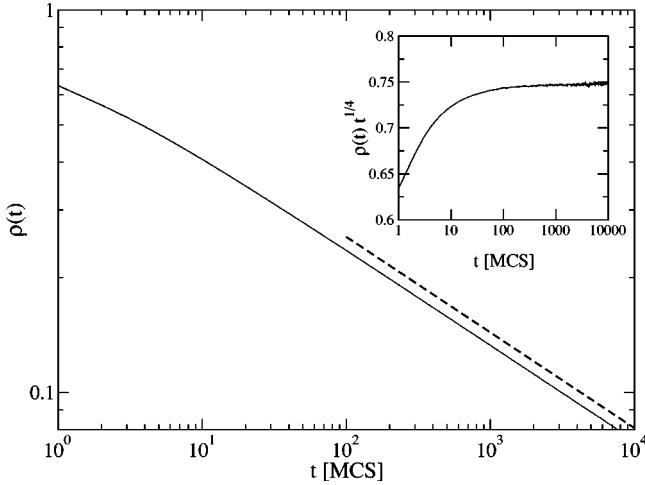


FIG. 9. Decay of the density of sites at zero height at the tricritical point $q=p=1$, $q_0=2/3$ as a function of time measured in Monte Carlo steps (MCS). The slope of the curve tends to $-0.24(1)$, leading to the conjecture that $\rho(t) \sim t^{-1/4}$.

Assuming standard power law scaling, all these results can be combined in the scaling forms,

$$\begin{aligned}\tilde{h}(\epsilon, \delta, N, t) &= N^{1/2} F(t/N^2, \epsilon N^{3/2}, \delta N^{1/2}), \\ \rho_0(\epsilon, \delta, N, t) &= N^{-1/2} G(t/N^2, \epsilon N^{3/2}, \delta N^{1/2}),\end{aligned}\quad (49)$$

where F and G are scaling functions with an appropriate asymptotic behavior. Again these scaling forms are consistent with the critical exponents $z=2, \alpha=1/2$ of the Edwards-Wilkinson universality class.

IV. MEAN-FIELD THEORY FOR NONEQUILIBRIUM WETTING

Mean-field theories describe a system in an approximate way by ignoring spatial correlations. For a given model there are many possible types of mean-field theories, depending on the microscopic level one is trying to describe. Previous mean-field approaches to nonequilibrium wetting considered the average height as the dynamical variable and studied the mean-field approximation of its dynamics. For example, in a study by Giada and Marsili [13] KPZ equation (5) was mapped by a Hopf-Cole transformation to a Langevin equation with multiplicative noise, discretizing space and replacing nearest-neighbor interactions by global couplings. Using a Morse potential with a potential well at zero height, they were able to reproduce second- and first-order transitions as well as phase coexistence. More recently, Santos *et al.* [14] extended these studies, suggesting that the mean-field phase diagram does not change if fluctuations are taken into account. Moreover, they identified a narrow domain close to the borderline between the phase coexistence region and the wet phase, where the system exhibits spatiotemporal intermittency.

In this section, we construct mean-field equations describing the temporal evolution of the height distribution ψ_n for height $h=n$. This approach is expected to yield more de-

tailed information on the structure of the interface than previous mean-field theories.

A. Mean-field equations

In order to construct the mean-field equations for the height distribution, let us first consider the case of a freely evolving interface without a wall. The rate equations describing the temporal change of ψ_n consist of several terms corresponding to different processes. Let us, for example, consider the probability that an attempted update leads to the desorption of an atom from the interior of a plateau at level n . This probability is proportional to ψ_n , which is the probability to find a randomly selected site at height n . Moreover, it depends on the heights of the nearest neighbors, which are restricted to take the values $\{n-1, n, n+1\}$. For simplicity, we assume that each site has two nearest neighbor sites. Clearly one can generalize it to the case where each site has $2(d-1)$ nearest neighbors. In this case one may have several types of edges of corner sites, requiring a larger number of growth rate parameters. To avoid this complication, we restrict ourselves to the case of two nearest neighbors. Thus, neglecting spatial correlations, the probability to find the two nearest neighbor sites at the heights $l, m \in \{n-1, n, n+1\}$ is assumed to be proportional to $\psi_l \psi_m$ divided by $(\psi_{n-1} + \psi_n + \psi_{n+1})^2$. For example, for evaporation from a plateau we have $n=l=m$ and thus the contribution of process (10) to the dynamical equation of ψ_n is

$$-p \frac{\psi_n^3}{(\psi_{n-1} + \psi_n + \psi_{n+1})^2}. \quad (50)$$

Similarly the loss of probability due to evaporation at edges (9) is given by

$$- \frac{2\psi_n^2 \psi_{n-1} + \psi_n \psi_{n-1}^2}{(\psi_{n-1} + \psi_n + \psi_{n+1})^2}, \quad (51)$$

while the deposition process (8) leads to a loss term of the form

$$-q \frac{\psi_n^3 + 2\psi_n^2 \psi_{n+1} + \psi_n \psi_{n+1}^2}{(\psi_{n-1} + \psi_n + \psi_{n+1})^2}. \quad (52)$$

In addition, there are corresponding gain contributions at the neighboring levels such that the total probability is conserved. Collecting all terms, the mean-field equations can be written as

$$\frac{d\psi_n}{dt} = A_n - A_{n-1}, \quad (53)$$

where

$$\begin{aligned}A_n &= \frac{p\psi_{n+1}^3 + 2\psi_n\psi_{n+1}^2 + \psi_n^2\psi_{n+1}}{(\psi_n + \psi_{n+1} + \psi_{n+2})^2} \\ &\quad - q \frac{\psi_n^3 + 2\psi_n^2\psi_{n+1} + \psi_n\psi_{n+1}^2}{(\psi_{n-1} + \psi_n + \psi_{n+1})^2}.\end{aligned}\quad (54)$$

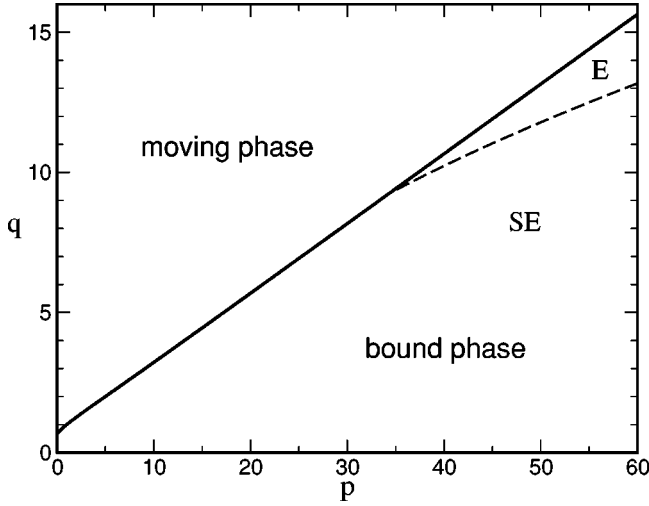


FIG. 10. Mean-field phase diagram for $q_0 = q$. The second-order phase transition line is represented as a solid line. The bound phase consists of two parts, where the interface profile ψ_n either decays exponentially (E) or superexponentially (SE) for large n .

The hard-core wall at the bottom layer can be taken into account by formally setting $\psi_{-1} = A_{-1} = 0$ and replacing q with q_0 in the expression for A_0 , which then can be written as

$$A_0 = \frac{p\psi_1^3 + 2\psi_0\psi_1^2 + \psi_0^2\psi_1}{(\psi_0 + \psi_1 + \psi_2)^2} - q_0\psi_0. \quad (55)$$

B. Mean-field phase diagram

The main result of the calculations, which will be presented in detail below, is the mean-field phase diagram shown in Fig. 10 for the case $q_0 = q$. As in the $(1+1)$ -dimensional model, there is a continuous phase transition from a bound to a moving phase. In calculating the mean-field height distribution in the moving phase, it is found that the interface is localized around its average height at any given time, representing a *smooth* growing interface. This is expected in high dimensions, for which mean-field represents a reasonable approximation. Clearly, in $d = 1 + 1$ dimensions this is not the case as discussed before.

In the bound region, two types of phases were found. In the larger part of the p, q plane (denoted as SE in Fig. 10), the height profile decays superexponentially at large height. In particular, it is found that for large n the profile takes the form

$$\psi_n \sim q^{-n} \exp(-2^{n-\alpha}), \quad (56)$$

where α is a constant. In addition, another region is found (denoted as E in Fig. 10), where the height distribution decays exponentially

$$\psi_n \sim e^{-an}, \quad (57)$$

where $a > 0$ is a constant.

The superexponential behavior may be understood by considering the equilibrium case (i.e., $p = 1$) in which a $(d - 1)$ -dimensional manifold is attracted by a gravitational force to a hard wall. The energy of a fluctuation reaching a height n scales as n^d , leading to the height distribution

$$\psi_n \sim e^{-\beta n^d}, \quad (58)$$

where $\beta > 0$ is a constant. This behavior seems to be valid in an extended nonequilibrium region of the phase diagram, as shown in Fig. 7, where numerical simulations in $d = 2 + 1$ dimensions are presented.

Numerical attempts to find signatures of a possible exponential phase in two and three dimensions failed since it is very difficult to obtain a reliable statistics in the tail of the height distribution, especially in higher dimensions, where finite-size effects become increasingly relevant. The conjecture that the exponential phase might be related to the roughening transition of KPZ interfaces in $d > 2$ could not be substantiated by numerical simulations.

C. Mean-field equations

In the stationary state, one has $A_0 = 0$ and $A_n - A_{n-1} = 0$ so that A_n vanishes for all $n \geq 0$. Therefore, the stationary mean-field equations read

$$0 = p\psi_1^3 + 2\psi_0\psi_1^2 + \psi_0^2\psi_1 - q_0\psi_0(\psi_0 + \psi_1 + \psi_2)^2, \quad (59)$$

$$0 = p\psi_{n+1}^3 + 2\psi_n\psi_{n+1}^2 + \psi_n^2\psi_{n+1} - q\psi_n(\psi_n + \psi_{n+1})^2 \times \left(\frac{\psi_n + \psi_{n+1} + \psi_{n+2}}{\psi_{n-1} + \psi_n + \psi_{n+1}} \right)^2, \quad (60)$$

where $n = 1, 2, \dots, \infty$. In order to solve this equation by iteration, it is convenient to consider quotients of successive densities,

$$x_n = \frac{\psi_n}{\psi_{n-1}}. \quad (61)$$

In terms of these variables, the stationary mean-field equations take the form

$$0 = px_1^3 + 2x_1^2 + x_1 - q_0(1 + x_1 + x_1x_2)^2, \quad (62)$$

$$0 = px_{n+1}^3 + 2x_{n+1}^2 + x_{n+1} - q(1 + x_{n+1})^2 \times x_n^2 \left(\frac{1 + x_{n+1} + x_{n+1}x_{n+2}}{1 + x_n + x_nx_{n+1}} \right)^2. \quad (63)$$

Bulk equation (63) can be interpreted as an iterative map $(x_n, x_{n+1}) \rightarrow (x_{n+1}, x_{n+2})$, where

$$x_{n+2} \equiv f(x_n, x_{n+1}) = -1 - \frac{1}{x_{n+1}} + \frac{1 + x_n + x_nx_{n+1}}{x_n(1 + x_{n+1})} \sqrt{\frac{1 + 2x_{n+1} + px_{n+1}^2}{qx_{n+1}}} \quad (64)$$

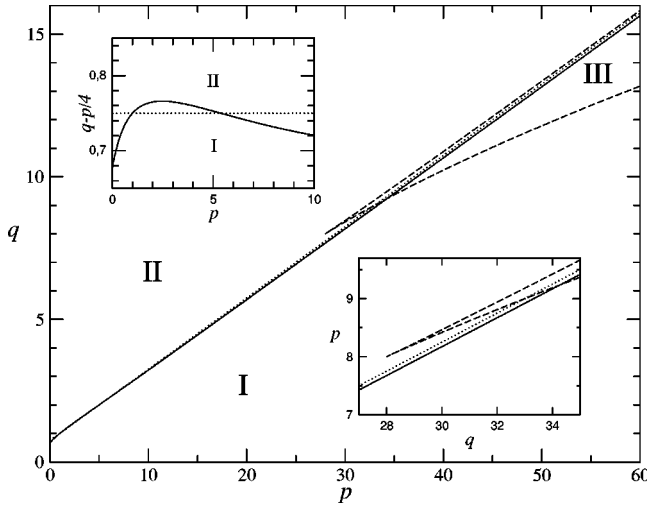


FIG. 11. Classification of fixed points depending on p and q . In region I (II), there exists only one real fixed point $x^* < 1$ ($x^* > 1$), while in region III there are three real fixed points. Regions I and II are separated by the straight dotted line $q = (p+3)/4$. The phase transition line (solid line) crosses from region I to region II and back into region I, as illustrated in the upper inset. The lower inset zooms the area where the both lines enter wedge-shaped region III.

for $n=1, 2, \dots, \infty$. In addition, the initial condition for x_1, x_2 is given by the bottom layer equation

$$x_2 = -1 - \frac{1}{x_1} + \sqrt{\frac{1 + x_1(2 + px_1)}{q_0 x_1}}. \quad (65)$$

D. Stationary solutions

In order to evaluate the stationary height distribution for given p and q , one has to look for a point on the line of possible initial conditions (65) and iterate map (64) such that it reaches a real fixed point with $x^* < 1$. This trajectory then corresponds to a physical height distribution.

To proceed, we first analyze the fixed points of the map. The fixed point equation

$$x[qx^3 + (2q-p)x^2 + (q-2)x - 1] = 0 \quad (66)$$

has four solutions. Two of the solutions $x_0^* = 0$ and x_1^* are real in the entire p, q plane, while other two solutions x_2^*, x_3^* may either be both real or complex conjugate to each other. We denote the region in the p, q plane, where x_2^*, x_3^* are real, by region III (see Fig. 11). We further divide the complementary region III into two regions; I, where $x_1^* < 1$, and II, where $x_1^* > 1$. Since the bracket in Eq. (66) is equal to -1 at $x=0$ and positive for $q>0$ in the limit of large x , the fixed point x_1^* has to be positive.

Analyzing map (64) with initial condition (65), we find that the only fixed points, which correspond to physical height distributions, are either x_0^* or x_2^* when it is real. Here x_2^* is the solution of Eq. (66) which satisfies $x_2^* < 1 < x_3^*$ in region III. In particular, we find that below the transition line, the height distribution is controlled by the fixed point x_0^*

$= 0$ in region I and by the fixed point x_2^* in region III. Details of the analysis, which led to this result, are given in the Appendix.

We now study the stationary height profile in the two regions. In region I the map flows to the hyperbolic fixed point $x_0^* = 0$ along its stable trajectory. Expanding the map for small values of x to lowest order, this stable manifold is described by the nonlinear relation

$$x_{n+1} \approx qx_n^2 \quad (67)$$

in the limit $x \rightarrow 0$. Along this manifold, the map approaches the fixed point $x_0^* = 0$ superexponentially as

$$x_n \approx \frac{1}{q} \exp(-2^{n-\alpha}) \quad (68)$$

yielding the height profile in Eq. (56).

In region III, stationary solutions are controlled by the fixed point $x_2^* > 0$ (see the Appendix). Linearizing the map around this fixed point one obtains an exponential behavior,

$$x_n \sim e^{-an}, \quad (69)$$

where $a > 0$ is a constant, leading to the exponential height profile (57).

To complete the analysis of the phase diagram, one has to locate the wetting transition line. This is done by simulating the dynamical mean-field equations (53) and determining the point from where on the interface detaches. This analysis leads to the transition line shown in Fig. 10.

So far all mean-field results were obtained for $q_0 = q$, i.e., without an attractive force between the substrate and wetting layer. Lowering q_0 changes the bottom layer equation (65) and thereby the possible starting points of the iteration. As shown in the Appendix, the mean-field approximation reproduces the phenomenon of phase coexistence. However, unlike in the model in $(1+1)$ dimensions, it emerges everywhere along the phase transition line as soon as $q_0 < q$; hence, there is no tricritical point. Moreover, in the limit $q_0 \rightarrow 0$ the threshold for the growth rate q , where the interface detaches, tends to infinity. Therefore, the region of phase coexistence is not bounded from above as in the $(1+1)$ dimensional model.

V. CONCLUSIONS

In this paper we have given a detailed account of a recently introduced solid-on-solid model for nonequilibrium wetting, which is defined in the spirit of a KPZ equation in a potential. Introducing a hard-core wall at zero height, the model exhibits a continuous wetting transition from a bound to a moving phase. The model is controlled by two parameters p and q , which effectively determine the asymptotic slope of the potential and the coefficient of the nonlinear term in the KPZ equation.

For $p=1$ the dynamical rules of the model obey detailed balance. In this case, the stationary distribution of a bound interface is given by a Boltzmann ensemble, which allows one to derive various quantities exactly. Moving away from

this line, the model crosses over to a nonequilibrium behavior, which is characterized by different critical properties. The model can be generalized further by including an attractive interaction between the substrate and the wetting layer. If this force is strong enough it may turn the continuous transition into a discontinuous one. Moreover, the bound and the moving phase may coexist in regions where the coefficient of the nonlinear term in the KPZ equation is negative.

In order to assess the behavior of the model in higher dimensions, we have proposed a mean-field approximation, which is based on rate equations for the densities at different heights. The phase diagram turns out to be surprisingly rich. It turns out that the mean-field approximation reproduces the properties of the original model. However, in the moving phase the interface remains smooth as it is expected for KPZ-type growth in higher dimensions.

As a new feature, the mean-field approximation predicts the existence of two different regions in the bound phase. In one of these regions the interface profile decays superexponentially with increasing height while in the other region an exponential decay is observed. This can be explained by classifying the fixed points of an iterative map for quotients of the densities. The question to what extent this crossover from superexponential to exponential profiles can be observed in the full model is still open.

ACKNOWLEDGMENTS

The support of the Israel Science Foundation (ISF) and the Einstein Center of the Minerva Foundation is gratefully acknowledged. The simulations were partly performed on the ALiCE parallel computer at the IAI in Wuppertal. H.H. would like to thank the INFN and the Weizmann Institute, where parts of this work were done, for hospitality.

APPENDIX: STATIONARY SOLUTIONS OF THE MEAN-FIELD EQUATIONS

1. Fixed points

Besides $x_0^*=0$, Eq. (66) has three other fixed points which are the roots of the polynomial equation

$$qx^3 + (2q-p)x^2 + (q-2)x - 1 = 0. \quad (\text{A1})$$

As shown in Fig. 11, the p,q plane can be divided into three different regions. In regions I and II, one fixed point is real and two of them are complex conjugate, while in region III all fixed points are real. The boundary of region III is characterized by the existence of a twofold degenerate fixed point. Comparing Eq. (A1) with a polynomial of the form $(x-a)^2(x-b)=0$, the boundary of region III can be given in a parameter representation by

$$q = \frac{2}{a-a^2}, \quad p = \frac{1+3a+4a^2}{a^2-a^3}, \quad b = \frac{1-a}{2a}, \quad (\text{A2})$$

where $0 < a < 1$. The boundary has the form of a wedge, shown as a dashed line in Fig. 11. The lower branch for $0 < a < 1/2$ and the upper branch for $1/2 < a < 1$ terminate in

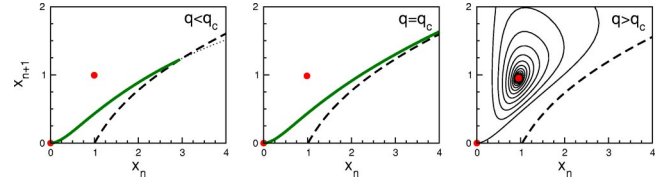


FIG. 12. Stationary solutions in region I: Superstable manifold of the fixed point $x_0^*=0$ for $p=2$ and different values of q in regions I and II. For $q < q_c$, the manifold (bold line) intersects the dashed line of possible initial conditions (65), representing a stationary solution in the bound phase, where the bottom layer density ψ_0 is positive. Approaching q_c , this intersection point moves to infinity and ψ_0 tends to zero. For $q > q_c$, the superstable manifold originates in the other real fixed point so that no stationary solution exists. Similar graphs are also obtained for other values of p in regions I and II.

the triple point $(p,q)=(8,28)$, where Eq. (A1) has a threefold degenerate fixed point $x^*=1/2$.

Physically meaningful stationary solutions of the iterative map must start from a point on the line given by Eq. (62) and have to flow towards a real fixed point with $0 \leq x^* < 1$. For this reason, we divided the complement of region III into two parts, namely, region I with $x_1^* > 1$ and region II with $x_1^* < 1$. Both regions are separated by a straight line $q=(p+3)/4$, where $x_1^*=1$.

2. Stationary solutions in regions I and II

We first show that in regions I and II a physically meaningful stationary solution always flows to the fixed point $x_0^*=0$. To this end we show that the other real fixed point x_1^* is either larger than 1 or unstable.

As shown in the upper inset of Fig. 11, the phase transition line starts at $p=0$ in region I, crosses into region II at the point $q=p=1$, and then crosses back into region I at the point $(p,q) \approx (5.380, 2.095)$. Obviously, the fixed point x_1^* can only be physically meaningful between these two crossing points, where $x_1^* < 1$. However, in this interval x_1^* turns out to be unstable. To demonstrate this point we consider the eigenvalues of the Jacobian of the map $x_{n+2}=f(x_n, x_{n+1})$ in Eq. (64),

$$\lambda_{1,2} = \frac{1}{2} \left(\frac{\partial f}{\partial x_{n+1}} \pm \sqrt{\left(\frac{\partial f}{\partial x_{n+1}} \right)^2 + 4 \frac{\partial f}{\partial x_n}} \right) \Bigg|_{x_n=x_{n+1}=x^*}. \quad (\text{A3})$$

Using Eq. (A1), the partial derivatives can be expressed as

$$\begin{aligned} \frac{\partial f}{\partial x_n} \Bigg|_{x_n=x_{n+1}=x^*} &= -\frac{1}{x^{*2}}, \\ \frac{\partial f}{\partial x_{n+1}} \Bigg|_{x_n=x_{n+1}=x^*} &= \frac{qx^{*4} + 2qx^{*3} + 2(q-1)x^{*2} + (3q-2)x^* - 2}{2qx^{*3}(x^*+1)}. \end{aligned} \quad (\text{A4})$$

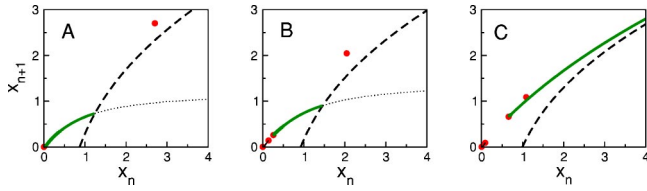


FIG. 13. Fixed points (bullets) and possible stationary solutions (bold lines) for $p=60$ inside for (a) $q=12.0$, (b) $q=13.5$, and (c) $q=q_c \approx 15.644$. The figure is explained in the text.

Along the dotted line in Fig. 11, where $x^*=1$, the two eigenvalues

$$\lambda_{1,2}|_{x^*=1} = 1 - \frac{1}{4q} (3 \pm \sqrt{9 - 24q}) \quad (\text{A5})$$

are complex conjugate in the interval between the two crossing points $1 < q < 5.380$. As can be verified numerically, they are also complex conjugate in a neighborhood of this line, which includes the phase transition line. Since the determinant of the Jacobian

$$\lambda_1 \lambda_2 = \frac{1}{x^{*2}} \quad (\text{A6})$$

is larger than 1 for $x^* < 1$, the fixed point x_1^* is found to be unstable. Thus we can conclude that physically meaningful stationary solutions in regions I and II are always controlled by the fixed point $x_0^*=0$.

Since for $x^* \rightarrow 0$ the two eigenvalues tend to $\lambda_1=0$ and $\lambda_2=-\infty$, the fixed point $x_0^*=0$ is nonlinear and hyperbolic. It has superstable manifold which in the limit of $x \rightarrow 0$ is given by $x_{n+1} = qx_n^2$. This manifold is shown in Fig. 12 for different values of q below, at, and above the critical point. As it can be seen, a stationary solution exists if the manifold intersects the line of possible initial conditions (65).

3. Stationary solutions in region III

In the wedge-shaped region III, there are three real fixed points $x_1^* < x_2^* < x_3^*$. The first one is smaller than 1 and unstable, while the second one is smaller than 1 and hyperbolic. The properties of x_3^* depend on p and q . Below the dotted line in Fig. 11, it is larger than 1 and stable, while it is smaller than 1 and unstable above.

Figure 13 illustrates typical situations at $p=60$ for various values of q , crossing region III from bottom to top. Below the wedge in region I [panel (a)], the stationary solution can

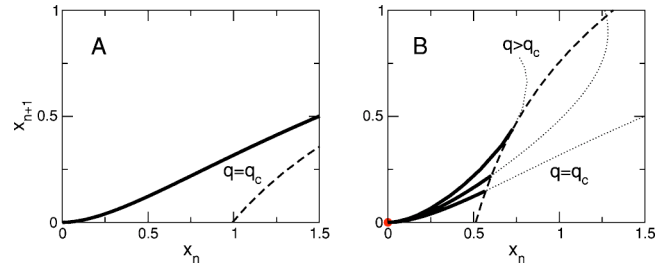


FIG. 14. Phase coexistence in the mean-field approximation for $p=0.8$ (see text).

be constructed in the same way as before. Entering region III from below [panel (b)], two new real fixed points $x_1^* < x_2^* < 1$ emerge, which are fully unstable and hyperbolic, respectively. The superstable manifold of the fixed point $x_0^*=0$ now originates in x_1^* , while it is the linearly stable manifold of the hyperbolic fixed point x_2^* which intersects the dashed line of possible initial conditions (65). As before, the intersection point moves continuously to infinity as q approaches the critical point [panel (c)]. Thus the unbinding transition manifests itself in the same way as in regions I and II, the only difference being that the physically relevant stable manifold is now controlled by the hyperbolic fixed point $x_2^* > 0$ instead of $x_0^*=0$. The linear stability of x_2^* is responsible for the purely exponential profile observed in region E.

4. Phase coexistence in regions I and II

Lowering q_0 changes the line of possible initial conditions (65), while the stable manifold of the fixed point $x_0^*=0$ remains the same. The typical situation for $p=0.8$ is shown in Fig. 14. The left panel shows the stable manifold (solid line) and the bottom layer equation (dashed line) without attractive force at the critical point $q_0=q=q_c \approx 0.943$. Both curves approach each other smoothly and intersect at infinity so that the transition is continuous. The right panel shows the same situation in the presence of an attractive force for $q_0=0.5$. Accordingly, the effect of lowering q_0 is to move the dashed line of possible initial conditions upward such that it intersects the critical stable manifold at a certain finite point. This means that the bottom layer density ψ_0 is finite at the critical point, making the transition first order. Moreover, a stationary solution still exists even if q is increased, proving the possibility of phase coexistence in the mean-field equations. Increasing q beyond a certain threshold, a stationary solution no longer exists. This defines the upper boundary of the phase coexistence region in the mean-field phase diagram.

- [1] S. Dietrich, in *Phase Transitions and Critical Phenomena*, edited by C. Domb and J.L. Lebowitz (Academic Press, London, 1986), Vol. 12, p. 1.
 [2] H. Nakanishi and M.E. Fisher, *Phys. Rev. Lett.* **49**, 1565 (1982).
 [3] D.S. Fisher and D.A. Huse, *Phys. Rev. B* **32**, 247 (1985); D.M. Kroll and R. Lipowsky, *ibid.* **26**, 5289 (1982); E. Brézin, B.I.

- Halperin, and S. Leibler, *Phys. Rev. Lett.* **50**, 1387 (1983).
 [4] A.-L. Barabási and H.E. Stanley, *Fractal Concepts in Surface Growth* (Cambridge University Press, Cambridge, 1995).
 [5] Y. Tu, G. Grinstein, and M.A. Muñoz, *Phys. Rev. Lett.* **78**, 274 (1997); M.A. Muñoz and T. Hwa, *Europhys. Lett.* **41**, 147 (1998).
 [6] U. Alon, M.R. Evans, H. Hinrichsen, and D. Mukamel, *Phys.*

- Rev. Lett. **76**, 2746 (1996); U. Alon, M.R. Evans, H. Hinrichsen, and D. Mukamel, Phys. Rev. E **57**, 4997 (1998); H. Hinrichsen, e-print cond-mat/0209179.
- [7] H. Hinrichsen, R. Livi, D. Mukamel, and A. Politi, Phys. Rev. Lett. **79**, 2710 (1997).
- [8] H. Hinrichsen, R. Livi, D. Mukamel, and A. Politi, Phys. Rev. E **61**, R1032 (2000).
- [9] A.L. Toom, in *Multicomponent Random Systems*, edited by R. L. Dobrushin, Advances in Probability Vol. 6 (Dekker, New York, 1980), pp. 549–575.
- [10] C.H. Bennett and G. Grinstein, Phys. Rev. Lett. **55**, 657 (1985).
- [11] C. Godrèche, J.M. Luck, M.R. Evans, D. Mukamel, S. Sandow, and E.R. Speer, J. Phys. A **28**, 6039 (1995).
- [12] R. Müller, K. Lippert, A. Kühnel, and U. Behn, Phys. Rev. E **56**, 2658 (1997).
- [13] L. Giada and M. Marsili, Phys. Rev. E **62**, 6015 (2000).
- [14] F. de Los Santos, M.M. Telo da Gama, and M.A. Muñoz, Europhys. Lett. **57**, 803 (2002); F. de Los Santos, M.M. Telo da Gama, and M.A. Muñoz, Phys. Rev. E **67**, 021607 (2003).
- [15] J. Candia and E.V. Albano, Eur. Phys. J. B **16**, 531 (2000); J. Phys.: Condens. Matter **14**, 4927 (2002); Phys. Rev. Lett. **88**, 016103 (2002).
- [16] F. Ginelli, V. Ahlers, R. Livi, A. Pikovsky, A. Politi, and A. Torcini, e-print cond-mat/0302588.
- [17] J.M.J. van Leeuwen and H.J. Hilhorst, Physica A **107**, 318 (1981).
- [18] T.W. Burkhardt, J. Phys. A **14**, L63 (1981).